MASTER'S DEGREE THESIS

Master of Science in Advanced Mathematics and Mathematical Engineering

Title: Mathematical and Numerical Models for Membrane Filtration Processes

Author: Jeremy Grant

Advisor: Marco Discacciati

Department: Departament de Matemàtica Aplicada III

Academic year: 2012

Facultat de Matemàtiques i Estadística

UNIVERSITAT POLITÈCNICA DE CATALUNYA

Abstract

This project concerns the effects of membrane fouling on membrane filtration operations.

Membrane filtration is a technique used to selectively separate particles from a fluid, typically either for the recovery of valuable components or for purifying the fluid. Many industrial applications (wastewater treatment, food processing, pharmaceutical production, etc.) rely on this general mechanism. An "idealized" membrane filtration system allows the solvent fluid to pass through while rejecting any particles having a size larger than the pore size of the membrane. This provides two output streams: the filtered solvent on one side of the membrane, and the removed solute on the other side.

However, in any real membrane filtration system, several physical phenomena interfere with the "ideal" operation described above. These include pore constriction, pore blocking, concentration polarization, and cake-layer formation. Each of these factors produces a reduction in the filtrate flow rate (if operating at constant pressure) or an increase in the transmembrane pressure (if operating at constant flux).

In this project, a model for the "idealized" membrane system is presented, using a Stokes model for the free-flow region and a Darcy model for the porous-media (membrane) region. The modes of membrane fouling described above are then considered, and two mathematical models (Wu *et al*. (2011) and Giraldo and LeChevallier (2006)) for these fouling effects are presented. Each model has its benefits, so a "combined" model is ultimately chosen. A description of how to implement this combined model numerically is provided, along with some numerical simulation results for a simple test case.

Finally, some possible further extensions to the model are briefly described.

Nomenclature

Symbol	Definition	Units
A	Available membrane surface area	m^2
A^0	Initial available membrane surface area (pre-fouling)	m^2
b	Cake resistance consolidation constant	m^3 / kg^2
C_c	Concentration of colloidal material in the bulk liquid	g / L
C_s	Concentration of soluble particles in the bulk liquid	g / L
$C_{s,mem}$	Concentration of soluble particles at the membrane surface	g / L
C_{ss}	Concentration of suspended solids in the bulk liquid	g / L
d	Cake compressibility coefficient	
D	Diffusion coefficient of given component	m^2 / s
f	Body forces per unit volume acting on the fluid	N / m^3
g	Fraction of suspended solids that form cake	
H	Height of flow channel	m
J_L	Local filtration flux	m / s
k	First-order particle removal coefficient	
K	Membrane hydraulic conductivity	m / s
m	Empirical constant	
n	Empirical constant	
p_f	Fluid pressure in the free-flowing region	Pa
p_p	Fluid pressure in the porous-medium region	Pa
P	Transmembrane pressure	Pa
ΔP_{cake}	Pressure drop across the cake	Pa
Q	Filtration rate	m^3 / s
Q^0	Initial filtration rate (pre-fouling)	m^3 / s
$r_{particle}$	Particle radius	m
r_{pore}	Membrane pore radius	m
R_{cake}	Cake resistance	m^{-1}
R_m	Intrinsic resistance of the membrane (pre-fouling)	m^{-1}
$R_{m,c}$	Membrane resistance (including pore constriction)	m^{-1}
R_T	Total resistance of the membrane (including fouling)	m^{-1}
R'	Specific cake resistance	m / kg
R''	Unit cake resistance	m^{-2}
R''_{comp}	Unit cake resistance (considering compressibility)	m^{-2}
t	Time	s
Δt	Time increment	s
T	Deviatoric stress tensor	
v_{air}	Scouring air surface velocity	m / s
v_f	Fluid velocity in the free-flowing region	m / s
$v_{f,x}$	Component of the free-flow fluid velocity in the x-direction	m / s
$v_{f,y}$	Component of the free-flow fluid velocity in the y-direction	m / s
x	Direction along the membrane	m
y	Direction perpendicular to the membrane	m
z_{cake}	Thickness of the cake layer	m
α	Pore blocking parameter	m^2 / kg
α_{BJ}	Constant for the Beavers-Joseph boundary condition	
α_f	Membrane porosity reduction coefficient	
α_p	Membrane pore reduction coefficient	

Symbol	Definition	Units
α_v	Air scouring coefficient	
β	Pore constriction parameter	kg
Γ	Boundary between the free-flow and porous-medium regions	
δ_m	Effective thickness of the membrane	m
λ	Dimensionless distance perpendicular to the membrane	
μ	Dynamic viscosity of the fluid	kg / m s
φ_{cake}	Cake porosity	
φ_m	Membrane porosity	
ρ	Fluid density	kg / m^3
ρ_{cake}	Cake density	kg / m^3
θ	Pore tortuosity	
τ_j	Unit vectors tangent to the boundary between subdomains	
Ω_f	Region where the fluid is flowing freely	
Ω_p	Region where the fluid is flowing through the membrane	

Table of Contents

1. Overview of Membrane Filtration and Fouling

Membrane filtration is a technique used to selectively separate particles from a fluid, typically either for the recovery of valuable components or for purifying the fluid. Many industrial applications (wastewater treatment, food processing, pharmaceutical production, etc.) rely on this general mechanism, which is often further classified into microfiltration, ultrafiltration, and nanofiltration (in order of decreasing membrane pore size) (American Water Works Association, 2005). Although different combinations of states can be used in membrane filtration systems, the majority of applications involve the separation of solid particles from a liquid stream (Vesilind *et al*., 1994), so that case will be considered here.

In an idealized membrane filtration system, the membrane is considered to be semi-permeable, allowing the solvent to pass through while rejecting any particles having a size larger than the pore size of the membrane. This ideal system would then provide two output streams: the filtered solvent on one side of the membrane, and the removed solute on the other side. By selecting a membrane with the appropriate pore size, the operator of the system could ensure a perfect separation of the desired and undesired streams (Vesilind *et al*., 1994).

However, in any real membrane filtration system, several physical phenomena interfere with the "ideal" operation described above. These include pore constriction, pore blocking, concentration polarization, and cake-layer formation (Beicha and Zaamouche, 2009). Each of these factors produces a reduction in the filtrate flow rate (if operating at constant pressure) or an increase in the transmembrane pressure (if operating at constant flux), so operators generally implement techniques to minimize them (Fitzgerald, 2008). The phenomena are described briefly below.

1.1 Fouling phenomena

The first major effect of membrane fouling, pore constriction, occurs when particles are deposited on the walls of the membrane pores, reducing the overall pore volume and increasing the resistance to flow. The particles are small enough to enter the pore, but once inside, they adhere chemically to the membrane material (membranes are typically chosen such that they are as inert as possible with respect to the fluid stream and

its components, but a certain amount of chemical interaction on the surface of the pores is unavoidable) (Environmental Dynamics Inc., no date). This adsorption may occur anywhere along the length of the pore, and is typically irreversible (although in some cases, chemical cleaning may be possible). Note that for pore constriction, the number of available pores remains constant, but the volume of the individual pores is reduced. This phenomenon is also sometimes known as pore adsorption (Broeckmann *et al*., 2006).

Note that in a related unit operation, known as clarification or filter-medium filtration, pore adsorption is the desired method of separation: the system is designed such that the particles will be trapped inside the pore structure of the filter (common clarification filters include cartridges or granular beds of sand or anthracite coal) (Millipore Corporation, 2003).

In contrast, the effect of the second major fouling mode, pore blocking, is to reduce the number of available pores. This effect is observed for particles having a diameter approximately equal to the pore diameter; the particles almost pass into the pore, but then become trapped in the opening, ensuring that no flow can occur through that pore (Chang *et al*., 2002; Vela *et al*., 2009).

As the solvent permeates through the membrane, a gradual increase in the concentration of non-permeating or slowly-permeating particles will occur on the feed side of the membrane. This concentration polarization results in a layer of fluid near the feed-side membrane surface in which the concentrations of the permeating substances are lower than their bulk concentrations, but the concentrations of non- or slowly-permeating substances are higher than their bulk concentrations (Pinto *et al*., 2010). The properties of this polarized layer have been the subject of considerable research (for example, Cath *et al*., 2006; Giraldo and LeChevallier, 2006; Huang and Morrissey, 1999; Song, 1998). It has been shown that the polarization increases the resistance to the flow of the solvent, and hence also reduces the permeate flux. In practice, this effect is often reduced by promoting turbulent mixing at the membrane surface (for example, by increasing the fluid velocity or adding turbulence-promoting screens, spacers, or baffles to the configuration) (Vesilind *et al*., 1994).

The final major membrane-fouling mechanism, cake formation, refers to the presence of a solid-like, or gel, layer at the surface of the membrane. When concentration

polarization occurs as described above, particles accumulate at the surface, becoming increasingly compacted and dense over time. Depending on the properties and configuration of the system, the cake layer is typically removed periodically by backflushing (with air or liquid) or mechanical cleaning (Drews, 2010).

Note that it is possible to operate the system at a low enough flux (below the so-called *critical flux*) such that no cake formation occurs. The critical flux can be determined for a given system; however subcritical operation is often impractical because it would require unreasonably large membrane surface areas (Jeison and van Lier, 2006).

Also note that the cake will have a different composition and hence different filtration properties from the membrane itself. As a result, the cake will function as a "secondary membrane" or pre-filter, often capturing small particles that would otherwise have reached the membrane surface and contributed to pore constriction or pore blocking. It has been shown that the presence of a thin cake layer is beneficial to the system because of this "pre-filtering" effect, but that as cake thickness increases, the resistance of the cake becomes dominant and begins to limit the flux (Giraldo and LeChevallier, 2006).

Typically, the maximum thickness of the cake layer (i.e., the thickness just prior to removal by cleaning) is of the same order of magnitude, or one order of magnitude smaller, than the thickness of the membrane itself. For many common applications, membrane layers are between 50-300 μm thick, whereas cake thicknesses of 3-120 μm have been reported based on experimental observations (Broeckmann *et al*., 2006; Gaucher *et al*., 2002; Saleem *et al*., 2011; Vyas *et al*., 2000; Ye *et al*., 2005).

In summary, concentration polarization is generally observed for all sizes of particles (in the sense that larger particles will be more concentrated at the membrane surface, whereas smaller particles will be less concentrated at the membrane surface, relative to the bulk concentrations), whereas the other three phenomena involve particles having the following sizes (the examples mentioned here are for a typical wastewater treatment system):

- Pore constriction: $r_{particle} < r_{pore}$ (e.g., soluble material)
- Pore blocking: $r_{particle} \approx r_{pore}$ (e.g., colloidal material)
- Cake formation: $r_{particle} > r_{pore}$ (e.g., suspended solids)

In almost all common membrane filtration applications, it is known that these fouling factors have a significant impact on the performance of the system; as such, a membrane model must account for these effects (Chang *et al*., 2001; Kim *et al*., 2001). Prior to presenting such a model, we will begin by presenting a simplified model for an idealized system (that is, without the effects of fouling).

2. A Simple Model of Membrane Filtration (Without Fouling)

Membranes are characterized by their porosity (the fraction of the membrane that is void space) and pore diameter (the diameter of an individual pore, generally assumed to be cylindrical). These properties will vary somewhat within the membrane, but modern manufacturing techniques are sufficiently advanced that we can assume constant properties over a given membrane, especially at the initial time before filtration begins (as the system runs, these properties may take on different values along the membrane; at these later times, we often still want to use a single value, which we can then regard as an average over the entire membrane) (Vesilind *et al*., 1994).

To account for the fact that the pores are not entirely direct "straight" paths through the membrane, the membrane tortuosity is defined as the ratio of the average pore length to the membrane thickness (Alves and Coelhoso, 2004).

Membrane systems are usually modelled as coupled free flow and porous-media flow problems. The domain is divided into two subdomains Ω_f (representing the region where the fluid is flowing freely) and Ω_p (representing the region where the fluid is flowing through the porous media). In each subdomain, we can use an appropriate model to obtain the fluid velocity and pressure (Zunino, 2002).

2.1 Free-flow subdomain

In the free-flow domain Ω_f, a standard fluid-flow model such as the Navier-Stokes equations can be used:

$$\rho\left(\frac{\partial v_f}{\partial t} + v_f \cdot \nabla v_f\right) = -\nabla p_f + \nabla \cdot T + f$$

where ρ is the fluid density, v_f is the fluid velocity in the free-flow region, p_f is the fluid pressure in the free-flow region, T is the deviatoric stress tensor, and f represents the body forces per unit volume acting on the fluid.

To fully specify the system, the above equation should be accompanied by a statement of conservation of mass (continuity equation):

$$\frac{\partial \rho}{\partial t} + \nabla \cdot (\rho v_f) = 0$$

If the fluid is assumed to be Newtonian and incompressible, with a constant viscosity (this can be assumed for many liquids), the above equations simplify to the following (Donaldson *et al*., 1985):

$$\rho\left(\frac{\partial v_f}{\partial t} + v_f \cdot \nabla v_f\right) = -\nabla p_f + \mu \nabla^2 v_f + f$$

$$\nabla \cdot v_f = 0$$

where μ is the dynamic viscosity.

Note that in the case of creeping flow (Reynolds number much less than 1, with inertial forces negligible relative to viscous forces), the above equations can be further simplified (indeed linearized) to yield the Stokes equations (Vesilind *et al*., 1994):

$$\nabla p_f = \mu \nabla^2 v_f + f$$

$$\nabla \cdot v_f = 0$$

2.2 Porous-media subdomain

The most common model for the fluid flow in the porous-media domain Ω_p is Darcy's law (which is applicable for slow, viscous flow with Reynolds numbers up to approximately 10):

$$Q = \frac{PA}{R_T \mu}$$

where Q is the filtration rate (with dimensions of volume per time), P is the transmembrane pressure, A is the porous media (membrane) surface area, and R_T is the

total resistance of the porous media (membrane) (Donaldson *et al*., 1985). In this idealized model, the resistance R_T is taken to be the intrinsic resistance of the membrane (this value is typically available from the membrane manufacturer), as we are not yet considering any increased resistance due to fouling.

Note that by computing Q/A, we can obtain a Darcy fluid "velocity". This quantity is not the true velocity that would be experienced by a given fluid particle passing through the membrane structure, but is instead a macroscopic quantity representing the flow through a given cross-section (Discacciati and Quarteroni, 2009). In the filtration literature, this quantity is often known as the "local filtration flux" and denoted by J_L (Wu *et al*., 2011).

2.3 Coupling between the free-flow and porous-medium subdomains

The solutions (fluid velocities and pressures) obtained in each of the two subdomains must then be coupled using appropriate boundary conditions. Let Γ represent the interface between the two subdomains. Then suitable boundary conditions include the following (Discacciati and Quarteroni, 2009; Zunino, 2002):

- Conditions for the fluid velocities
  - for incompressible fluids, continuity of the normal component of the velocity at the interface:

    $$v_f \cdot n = J_L \cdot n \qquad \text{on } \Gamma$$

    where n is the unit outward normal vector to the surface $\partial\Omega_f$
  - in some cases, an additional condition for the tangential component of the velocity (such as a modified Beavers-Joseph condition):

    $$\frac{\mu\alpha_{BJ}}{\rho\sqrt{K}} v_f \cdot \tau_j - \tau_j \cdot T(v_f, p_f) \cdot n = 0 \qquad \text{on } \Gamma$$

    where K is the hydraulic conductivity of the membrane, α_{BJ} is a dimensionless constant, and τ_j (j = 1,2) are linearly-independent unit vectors tangent to the boundary Γ.
- Conditions for the fluid pressures

- typically, a Neumann-type condition balancing the pressures across the interface is used:

$$-n \cdot T(v_f, p_f) \cdot n = p_p \text{ on } \Gamma$$

where p_p is the fluid pressure in the porous-medium subdomain.

Note that the location of the boundary Γ between the two subdomains will not remain constant over time; rather, it will vary with the thickness (height) of the cake layer that is formed on the surface of the membrane (Jeison and van Lier, 2006). Because of the relatively dense structure of the cake, it should be considered as an extension of the porous-medium subdomain, rather than as part of the free-flow subdomain (we will see that the models described below treat the cake layer as a porous medium). As noted earlier, the cake-layer thickness can be of the same order of magnitude as the thickness of the membrane itself (or one order of magnitude smaller); thus, locating the boundary is a significant concern to ensure the accuracy of the model. Further details on determining the location of the boundary between the subdomains are given in section 3.4.

3. Incorporating Fouling Effects into the Model

The models introduced in the preceding section are suitable for an idealized membrane filtration system in which no fouling occurs. We can now introduce additional parameters to represent the effects of fouling.

Qualitatively, we can intuit that in the porous-media (membrane) subdomain Ω_p, fouling will have the effect of increasing the membrane resistance and reducing the available membrane surface area. As expected, we can see from Darcy's law that this will reduce the filtration rate and hence the local filtration flux J_L (if operating at constant pressure) or increase the transmembrane pressure (if operating at constant flux). Several models have been developed to quantify these fouling effects, using slightly different assumptions and reasoning, two of which are outlined below.

3.1 Wu, He, Jiang, and Zhang, 2011

This model was developed for the case of wastewater treatment in a membrane bioreactor (such systems are the most common configuration for wastewater treatment

worldwide). It assumes that cake formation (caused primarily by suspended solid particles), pore blocking (caused primarily by colloidal material), and pore constriction (caused primarily by soluble components) all occur simultaneously.

By considering the phenomena simultaneously, the model incorporates the "pre-filtering" effect of the cake (i.e., colloidal and soluble material can become trapped in the cake prior to reaching the membrane itself). This interaction has the obvious effect of reducing the available colloidal and soluble material for pore blocking and pore constriction; it also means that the cake itself will become more consolidated as the colloidal and soluble material bind the larger solid particles together (i.e., the cake resistance will increase).

The development of the cake resistance over time is given by:

$$\frac{dR_{cake}}{dt} = gR' J_L C_{SS}$$

where R_{cake} is the cake resistance, g is the fraction of suspended solids that form cake, R' is the specific cake resistance, C_{ss} is the suspended solids concentration, and J_L is the "local filtration flux":

$$J_L = \frac{Q(t)}{A(t)}$$

where $A(t)$ is the available membrane surface area at the particular time being considered (an equation for the available area is given below). Note that while J_L is called a "flux" in the literature, it has the units of velocity.

As mentioned, the specific cake resistance will not remain constant, but instead will increase over time as the cake layer traps colloidal and soluble material, which help to consolidate the cake and reduce its porosity:

$$\frac{dR'}{dt} = bJ_L(C_S + C_c)$$

where C_s and C_c are the soluble and colloidal component concentrations, respectively, and b is the cake resistance consolidation constant.

The available membrane surface area is given by:

$$\frac{dA}{dt} = \alpha QC_c \frac{m}{m + R_{cake}}$$

where α is a pore blocking parameter and m is an empirical constant. Note that this equation incorporates the concentration of colloidal material, which is responsible for the pore blocking that will reduce the available area. The term (m / (m+R_{ca})) describes the effect of the cake layer on the pore blocking – the cake layer will have a greater effect on pore blockage for low values of m, whereas a very high value of m would mean that the cake layer has no effect on pore blocking.

The remaining factor to be considered is pore constriction, which can be modelled by the following equation:

$$R_{m,c} = R_m\left(1 + \beta Q C_s \frac{n}{n + R_{cake}} t\right)^2$$

where $R_{m,c}$ is the total resistance of the membrane, R_m is the intrinsic resistance of the membrane (i.e., before any pore constriction has occurred), β is a pore constriction parameter, and n is an empirical constant. As expected, we see that the effect of pore constriction will be to increase the resistance of the membrane; we also see that the extent of constriction is dependent on the concentration of soluble particles (which are the ones expected to enter pores and adhere there, because of their small size). Again, the cake will act as a "pre-filter" for the soluble particles, and the term (n / (n+R_{cake})) describes the effect of the cake layer on the pore constriction – the cake layer will have a greater effect on pore constriction for low values of n, whereas a very high value of n would mean that the cake layer has no effect on pore constriction.

Combining all of the fouling phenomena, we can now compute the overall resistance as:

$$R_T = R_{m,c} + R_{cake}$$

This quantity, along with the available membrane surface area computed above, can then be inserted into Darcy's law to compute either the transmembrane pressure (for constant-flux operation) or the filtration rate (and hence the Darcy velocity, for constant-pressure operation) at any given time:

$$P = \frac{Q^0 R_T \mu}{A}$$

$$Q = \frac{A R_m}{A^0 R_T} Q^0$$

where Q^0 and A^0 represent the initial (pre-fouling) filtration rate and membrane surface area, respectively.

In order to implement this model, we need to solve the differential equations for cake resistance, specific cake resistance, and available surface area. This was done numerically by Wu *et al*. (2011) using first-order Taylor approximations:

$$R_{cake}(t+\Delta t) = R_{cake}(t) + gR'(t)J_L(t)C_{ss}\Delta t$$

$$R'(t+\Delta t) = R'(t) + bJ_L(t)(C_s + C_c)\Delta t$$

$$A(t+\Delta t) = A(t) - \Delta t\left(\alpha Q(t)C_c \frac{m}{m + R_{cake}(t)}\right)$$

$$J_L(t) = \frac{Q(t)}{A(t)}$$

Note that to solve the model, we need to provide values for six parameters (g, b, α, β, m, and n) and the initial specific cake resistance ($R'(0)$). Wu *et al*. (2011) reviewed experimental data for three membrane bioreactors with different aeration intensities, and used a least-squares method to evaluate the parameters. The range of their results are shown below.

Symbol	Definition	Range	Units
g	Fraction of suspended solids that contribute to cake formation	0.0101 – 0.0460	
b	Cake resistance consolidation constant	$1 \times 10^{15} – 3.5 \times 10^{15}$	m^3 / kg^2
α	Pore blocking parameter	71 – 282	m^2 / kg
β	Pore constriction parameter	$6.78 \times 10^3 – 1.4772 \times 10^4$	kg
m	Empirical constant	1×10^{16}	
n	Empirical constant	1×10^{10}	
$R'(0)$	Initial specific cake resistance	1×10^{10}	m / kg

Finally, note that while this model does not explicitly include the aeration rate in its equations, it has been tested and found to be effective over a range of aeration rates;

importantly, parameter values are available in the literature for at least three of the most common aeration rates.

3.2 Giraldo and LeChevallier, 2006

This model was also developed for the case of a membrane bioreactor in wastewater treatment. Like the model above, it considers the interaction between cake formation and "internal fouling" (i.e., pore blocking and pore constriction). As above, the model considers that larger particles will lead to cake formation, while smaller, soluble particles will contribute to pore constriction.

This model's approach is different in that it explicitly considers the change in effective pore radius and membrane porosity as fouling occurs. First, we introduce an equation for membrane resistance:

$$R_m = \frac{8\theta\delta_m}{\varphi_m r_{pore}^2}$$

where θ is the pore tortuosity, δ_m is the thickness of the membrane, φ_m is the membrane porosity, and r_{pore} is the effective pore radius.

θ and δ_m are properties of the membrane and are assumed to remain constant, even when fouling occurs. Qualitatively, we expect decreases in both the membrane porosity and the effective pore radius due to pore constriction and pore blocking. This model quantifies these effects as follows:

$$\frac{d\varphi_m}{dt} = -\alpha_f C_{s,mem} J_L$$

$$\frac{dr_{pore}}{dt} = -\alpha_p C_{s,mem} J_L$$

where $C_{s,mem}$ is the concentration of soluble particles at the membrane surface (as opposed to in the bulk liquid), α_f is the membrane porosity reduction coefficient, and α_p is the membrane pore reduction coefficient.

To quantify the rate of cake formation, a mass balance is performed. The change in cake mass over a given time will be the amount of material deposited in the cake from

the bulk liquid, minus the amount of material removed from the cake due to the air scouring (which is pushing material from the cake back into the bulk liquid):

$$\rho_{cake} \frac{dz_{cake}}{dt} = J_L C_{ss} - \alpha_v v_{air}$$

where ρ_{cake} is the density of the cake layer, z_{cake} is the thickness of the cake layer, α_v is an air scouring coefficient, and v_{air} is the scouring air surface velocity.

The cake resistance is then given by:

$$R_{cake} = R''_{comp} z_{cake}$$

where R''_{comp} is the cake resistance per unit thickness of cake (this quantity is sometimes called the "specific cake resistance" in the literature, but since we have already used that term in a different sense above, we will use "unit cake resistance" to refer to R''_{comp}). The subscript "*comp*" indicates that this quantity will take into account the compressibility of the cake. First, we will use the Kozeny-Carman equation to determine the unit cake resistance without considering compressibility (R''):

$$R'' = \frac{45(1-\varphi_{cake})^2}{r_{particle}^2 \varphi_{cake}^3}$$

where φ_{cake} is the porosity of the cake, and $r_{particle}$ is the effective mean radius of particles forming the cake. We now introduce an extra factor to account for the cake compressibility:

$$R''_{comp} = R'' \Delta P_{cake}^d$$

where ΔP_{cake} is the pressure drop across the cake and d is the cake compressibility coefficient, which has been experimentally determined to be in the range of 0.79 to 1.4 (note that if d is taken equal to zero, the cake is incompressible).

In the differential equations above for the membrane porosity and the effective pore radius, we need to use the concentration of soluble particles at the membrane surface (where pore constriction and pore blocking will actually occur) rather than in the bulk liquid. As discussed above, the cake will serve as a "pre-filter" for these particles, so the concentration at the membrane surface will be less than in the bulk liquid. This is

quantified as follows (this equation is derived by integrating the mass balance on an element in the cake):

$$C_{s,mem} = C_s e^{\frac{kz_{cake}}{J_L}}$$

where k is a first-order particle removal coefficient.

The differential equations for the membrane porosity, effective pore radius, and height of the cake layer can now be solved numerically. For example, using a first-order Taylor approximation:

$$\varphi_m(t + \Delta t) = \varphi_m(t) - \alpha_f C_{s,mem} J_L(t) \Delta t$$

$$r_{pore}(t + \Delta t) = r_{pore}(t) - \alpha_p C_{s,mem} J_L(t) \Delta t$$

$$z_{cake}(t + \Delta t) = z_{cake}(t) + (J_L(t) C_{ss} - \alpha_v v_{air}) \Delta t$$

As with the previous model, the total resistance (including the effects of pore constriction, pore blocking, and the cake layer) at any time can be computed (as the sum of R_m and R_{cake}) and inserted into Darcy's law to obtain the transmembrane pressure or the filtration rate (and hence the Darcy velocity), as appropriate.

3.3 Comparison of the models

Both of the models presented above use Darcy's law to evaluate the transmembrane pressure or filtration rate, but they differ in how they evaluate the decline in available membrane surface area and the increase in resistance due to fouling. The biggest strength of these models is that they are able to capture the interaction between the different modes of fouling; this represents a significant advantage over other models in the literature.

While both models were developed and tested for membrane bioreactor systems, it seems that they would be applicable to other membrane systems in which the same fouling mechanisms take place. The models are generally derived from fundamental principles, although each relies to a certain extent on empirically-derived constants that would be dependent on the specific system being modelled.

In fact, one significant drawback of the second model (Giraldo and LeChevallier, 2006) is that it relies on several parameters (α_f, α_p, α_v, and k) for which values are not readily available in the literature. Because of this concern, the first model (Wu *et al*., 2011) is a more suitable choice for the determination of the overall system resistance and then the transmembrane pressure (for constant flux operation) or the filtration rate (and hence the Darcy velocity, for constant pressure operation).

3.4 Combination of the models

Note that the first model does not provide an explicit method for calculating certain physical properties of the system (e.g., thickness of the filter cake and effective pore radius). The most significant of these is the filter cake thickness (height) z_{cake}, which is important because it indicates the location of the boundary Γ between the free-flow subdomain Ω_f and the porous-media subdomain Ω_p at any given time. Fortunately, by combining the two models, we can still compute z_{cake}.

To do this, we proceed with the first model as usual, using it to calculate the resistances (membrane, cake, and total), the available surface area, and the resulting local flux $J_L(t)$. We can then input this value, along with aeration information and the known concentration of suspended solids, into the second model's equation for the cake height.

$$z_{cake}(t+\Delta t) = z_{cake}(t) + (J_L(t)C_{ss} - \alpha_v v_{air})\Delta t$$

Then of course the interface Γ between the subdomains is located at a distance z_{cake} from the original membrane boundary.

Note that the above procedure is applicable even in the case of constant-flux operation (in this scenario, rather than a decrease in the flux $Q(t)$, we have an increase in the transmembrane pressure $P(t)$). Recall the equation for the "local filtration flux" (which in fact has units of velocity):

$$J_L = \frac{Q(t)}{A(t)}$$

In the constant-flux case, the numerator $Q(t)$ remains constant, but we still observe a decrease in the available surface area $A(t)$, so our values of $J_L(t)$, and hence the computed z_{cake}, remain accurate. Also note that in both the constant-flux and constant-

pressure cases, the local filtration flux J_L increases with time, indicating that the rate of growth of the cake layer will also increase with time.

4. Numerical Implementation of the Model

The numerical implementation of the model proposed by Wu *et al*. (2011) was discussed briefly in section 3.1. A more detailed discussion will be presented here, to illustrate how the system of ordinary differential equations and nonlinear algebraic equations can be solved to determine the filtration flux (for constant-pressure operation) or the transmembrane pressure (for constant-flux operation) for any given time.

4.1 Procedure for solving the system

First, we define the system to be solved, beginning with three ordinary differential equations for the cake resistance, specific cake resistance, and available membrane surface area, and then the algebraic equation for the membrane resistance:

$$\frac{dR_{cake}}{dt} = gR'(t)\frac{Q(t)}{A(t)}C_{SS}$$

$$\frac{dR'}{dt} = b(C_S + C_c)\frac{Q(t)}{A(t)}$$

$$\frac{dA}{dt} = \alpha Q(t)C_c\frac{m}{m + R_{cake}(t)}$$

$$R_{m,c}(t) = R_m\left(1 + \beta C_s n\frac{Q(t)}{n + R_{cake}(t)}t\right)^2$$

We must now specify a fifth equation. If the system is being operated at constant pressure, we add the following equation for the overall flux as a function of time:

$$Q(t) = \frac{A(t)Q^0R_m}{A^0(R_{m,c}(t) + R_{cake}(t))}$$

On the other hand, if the system is being operated at constant flux, we instead add the following equation for the transmembrane pressure as a function of time:

$$P(t) = \frac{Q^0R_T(t)\mu}{A(t)}$$

The constant-pressure case will be considered in detail here, but the procedure for the constant-flux case is very similar.

The unknowns in the system are R_{cake}, R', Q, A, and $R_{m,c}$, all of which are dependent on time. To approximate the solution, we will split the system into two parts: first we solve the subsystem of ordinary differential equations, then we address the two nonlinear algebraic equations. First, we must choose a suitable method of integrating the ordinary differential equations. For simplicity, we will consider the forward Euler method here, but in practice, other more advanced methods could be used to provide increased stability and reduced error.

We can begin by working with the three ordinary differential equations, in order to determine R_{cake}, R', and A. In the forward Euler scheme, the rate of change of a quantity X is approximated as follows:

$$\frac{dX}{dt} \approx \frac{X^{n+1} - X^n}{\Delta t}$$

where X^{n+1} and X^n are approximations of the value of X at subsequent times t_{n+1} and t_n, respectively, which are separated by an increment Δt. Thus, in this system, the ordinary differential equations can be integrated as follows:

$$\frac{R_{cake}^{n+1} - R_{cake}^n}{\Delta t} = C_{ss} g (R')^n \frac{Q^n}{A^n}$$

$$\frac{(R')^{n+1} - (R')^n}{\Delta t} = b(C_s + C_c)\frac{Q^n}{A^n}$$

$$\frac{A^{n+1} - A^n}{\Delta t} = -\alpha C_c m \frac{Q^n}{m + R_{cake}^n}$$

(Note that this method requires that we have values or estimates of the initial flux Q^0, initial cake resistance R^0_{cake}, initial specific cake resistance $(R')^0$, and initial membrane surface area A^0. Suitable estimates for these quantities are discussed in section 4.2.)

Having now computed the updated estimates $R^{n+1}{}_{cake}$, $(R')^{n+1}$, and A^{n+1}, we can then move to the algebraic equations, for which we can use a similar discretization approach:

$$Q^{n+1} = \frac{A^{n+1} Q^0 R_m}{A^0 (R_{m,c}^{n+1} + R_{cake}^{n+1})}$$

$$R_{m,c}^{n+1} = R_m \left(1 + \beta C_s n \frac{Q^{n+1}}{n + R_{cake}^{n+1}} \right)^2$$

Substituting the equation for $R_{m,c}{}^{n+1}$ into the expression for Q^{n+1}, we obtain the following:

$$Q^{n+1} = \frac{A^{n+1} Q^0 R_m}{A^0 \left(R_m \left(1 + \beta C_s n \frac{Q^{n+1}}{n + R_{cake}^{n+1}} \right)^2 + R_{cake}^{n+1} \right)}$$

This nonlinear algebraic equation can be solved using a standard routine such as the FZERO function in MATLAB. The local filtration flux and cake thickness can then be computed:

$$J_L^{n+1} = \frac{Q^{n+1}}{A^{n+1}}$$

$$z_{cake}^{n+1} = z_{cake}^{n} + (J_L^{n+1} C_{ss} - \alpha_v v_{air}) \Delta t$$

With the local Darcy velocity (J_L) and the location of the boundary between free-flow and porous-media subdomains (based on the cake thickness z_{cake}) now known, we can then couple these results with the free-flow regime, using the boundary conditions described in section 2.3.

4.2 Simulation results

A numerical implementation of the model was completed in MATLAB. The table below summarizes the parameters that were specified in order to solve the system.

Parameter	Value	Rationale
Intrinsic resistance of the membrane (pre-fouling), R_m	4×10^{11} m^{-1}	Average of values reported by Chang *et al*. (2002)
Initial available membrane surface area, A^0	100 m^2	
Initial flux, Q^0	1×10^{-4} m^3 / s	
Initial specific cake resistance, $(R')^0$	1×10^{10} m / kg	Wu *et al*. (2011)
Initial cake thickness, z^0_{cake}	0 m	At the initial time, no cake layer has formed yet
Concentration of suspended solids, C_{ss}	2.5 g / L	Representative value for wastewater (Hach, no date)
Concentration of soluble components, C_s	2.0 g / L	Representative value for wastewater (Wang, 2004)
Concentration of colloidal components, C_c	5.0 g / L	Representative value for wastewater (Wang, 2004)
Cake resistance consolidation constant, b	2.2×10^{15} m^3 / kg^2	Average of values reported by Wu *et al*. (2011)
Fraction of suspended solids that form cake, g	0.0267	Average of values reported by Wu *et al*. (2011)
Pore blocking parameter, α	160 m^2 / kg	Average of values reported by Wu *et al*. (2011)
Pore constriction parameter, β	1.095×10^4 kg	Average of values reported by Wu *et al*. (2011)
Air scouring coefficient, α_v	1×10^{-6}	Giraldo and LeChevallier (2006)
Scouring air surface velocity, v_{air}	0.4 m / s	Average of values reported by Chang *et al*. (2002)
Empirical modelling constant, m	1×10^{16}	Wu *et al*. (2011)
Empirical modelling constant, n	1×10^{10}	Wu *et al*. (2011)
Time increment, Δt	0.05 s	
Total run time	5 minutes	Representative of time between cleanings (Drews, 2010)

Using the results of this simulation, we can observe some general trends. However, we should note that the results may vary considerably depending on the value of each of the parameters specified above; in practice, these parameters must be carefully chosen to represent the membrane system being studied. The following figures show the specific cake resistance R', the cake resistance R_{cake}, the filtration rate Q, the available membrane surface area A, the local filtration flux J_L, and the cake thickness z_{cake} as functions of time.

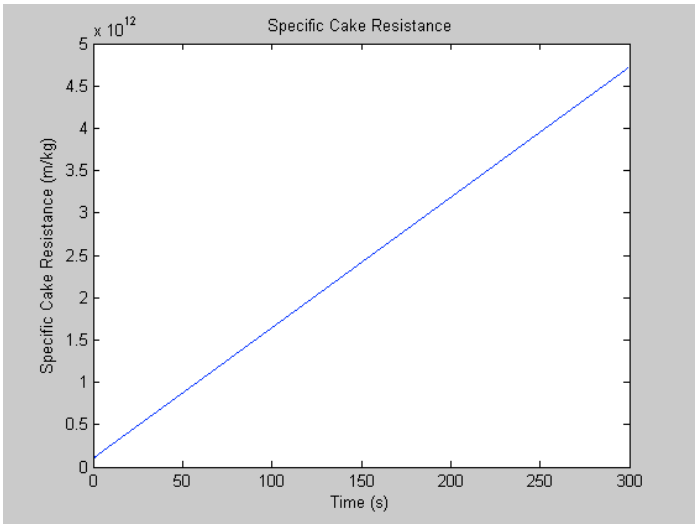
Specific Cake Resistance
x 10^12
Specific Cake Resistance (m/kg)
Time (s)

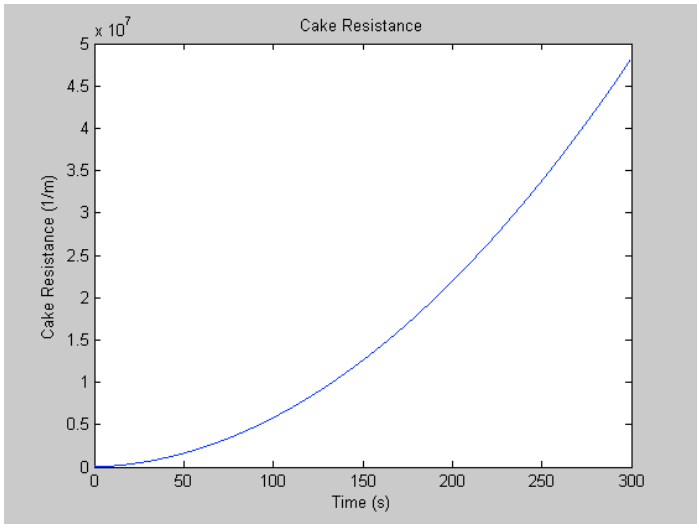
Cake Resistance
x 10^7
Cake Resistance (1/m)
Time (s)

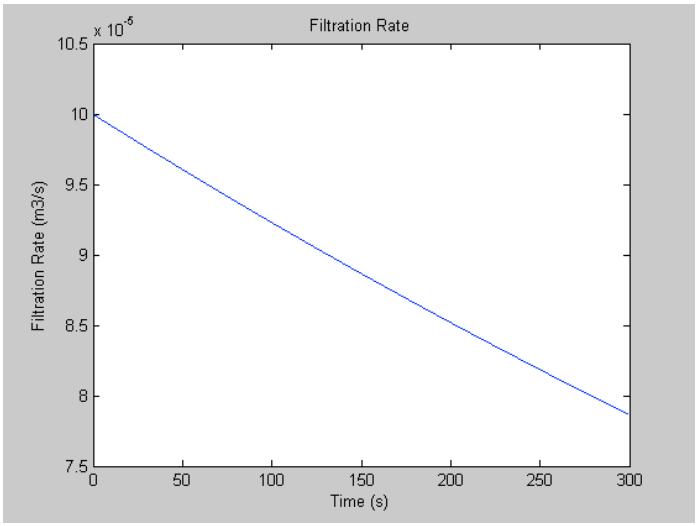
Filtration Rate
x 10^-5
Filtration Rate (m3/s)
Time (s)

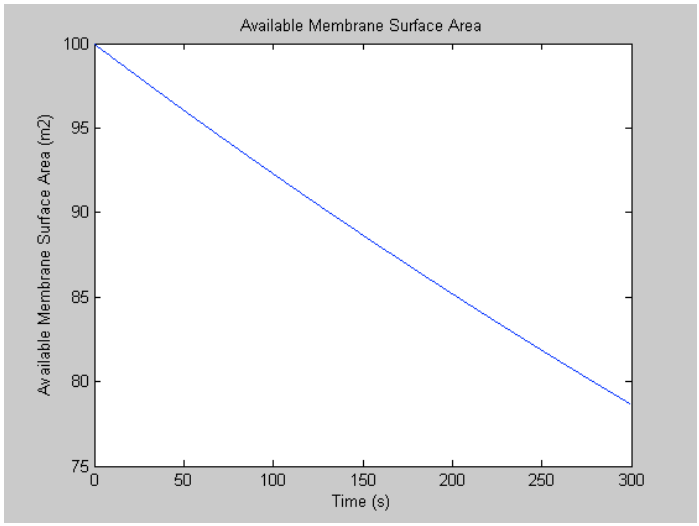
Available Membrane Surface Area
Available Membrane Surface Area (m2)
Time (s)

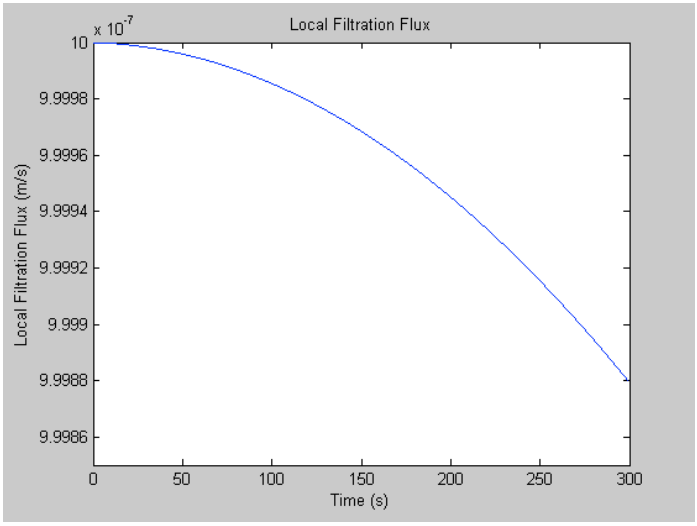
Local Filtration Flux
x 10^-7
Local Filtration Flux (m/s)
Time (s)

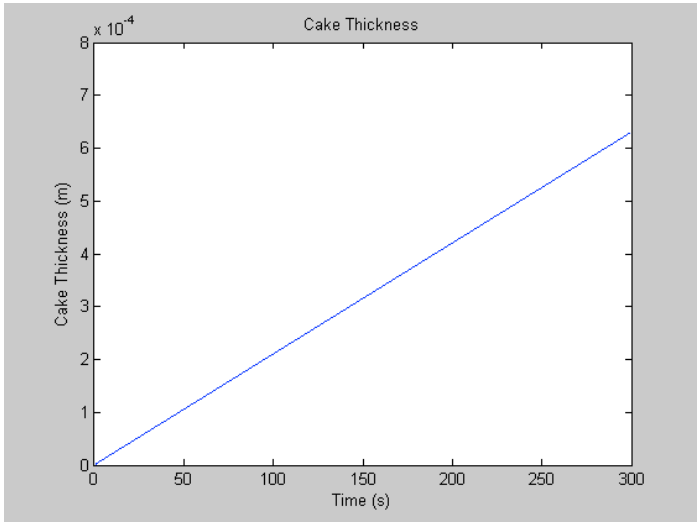
Cake Thickness
x 10^-4
Cake Thickness (m)
Time (s)

We observe that the specific cake resistance increases with time, as the cake becomes more compact. Similarly, the total cake resistance increases as the cake becomes both thicker and more compact. The filtration rate decreases as the solution becomes less able to pass through the combined membrane-cake porous medium. The available membrane surface area decreases as pores become blocked by the presence of the cake above. The local filtration flux (which represents the effective "velocity" of the fluid passing through the porous medium) decreases. The cake thickness increases as material continues to deposit.

The trends described above for specific cake resistance, total cake resistance, filtration rate, and available membrane surface area are each in agreement with those presented in Wu *et al*. (2011), although that paper did not include simulated results for the local filtration flux or the cake thickness.

Finally, note that the results described above represent the behavior of the system in the short term (roughly equivalent to the run time between cleanings). Readers interested in results over a longer time scale can refer to Wu *et al*. (2011).

5. Possible Extensions of the Model

In the membrane-fouling model presented above, the concentrations of suspended solids, soluble components, and colloidal components are considered to be constant, both in time and in each of the spatial dimensions. In addition, other parameters, such as the cake resistance, specific cake resistance, and local filtration flux, are considered as constants over space, and modelled with suitable "average" values. These assumptions simplify the computations considerably, but also introduce some inaccuracy into the model.

5.1 Variation of concentrations over time

In most membrane filtration systems, the concentration of each solute in the feed solution entering the filtration unit can generally be assumed to be constant (because this feed will typically come from another unit operation that produces a relatively consistent output stream), and represented in the model by a suitable "average" value. Throughout the filtration literature, it is often further assumed that these concentrations will remain

constant over a given run, as any changes in concentration will be minimal over each relatively short run time (in membrane systems, backflushing with a chemical cleaner typically occurs once every 3-12 minutes of filtration time (Drews, 2010), to avoid the formation of a thick and impenetrable cake layer). If desired, the model could be updated with new concentration values (if measurements or estimates are available) following each cleaning cycle.

Note that the time scale of pore blocking is much shorter – Song (1998) found that the time required for 99%-complete pore blocking was 4 to 6 orders of magnitude smaller than the time required for cake formation that would reduce the flux by 99% under the same operating conditions. As a result, unless the intent is to specifically study the microscopic mechanism of pore obstruction in a given system, there is no need to model the time-dependence of the pore blocking, as we can simply assume a steady state at which significant pore blocking has already occurred, and simulate the development of the cake layer from there.

The concentrations of suspended solids, soluble components, and colloidal components are used in the differential equations for the cake resistance, specific cake resistance, and available membrane surface area. If one or more of these concentrations were considered to be functions of time, these equations would become more complex; and a suitable model would need to be developed to express each of the non-constant concentrations as a function of time, to ensure that the system remained solvable.

5.2 Variation of concentrations and other parameters over space

In the current model, the concentrations of each component are taken to be a suitable "average" value in each of the spatial dimensions. If it is deemed important to model the variation of these concentrations in space, a diffusion-transport-reaction model, with appropriate boundary conditions, can be used. Typically, the movement of the components will be dominated by the transport term rather than diffusion, and in almost all cases the reaction term can be neglected.

Song (1998) used this type of model to describe the change in concentration of a given component in the direction perpendicular to the membrane, in order to study the effects of concentration polarization. Huang and Morrissey (1999) proposed a model

describing changes in concentration due to transport along the surface of the membrane (defined as the x direction) and both transport and diffusion in the direction perpendicular to the membrane (defined as the y direction):

$$v_{f,x}\frac{\partial C}{\partial x}+\frac{v_{f,y}}{H}\frac{\partial C}{\partial \lambda}=\frac{D}{H^2}\frac{\partial^2 C}{\partial \lambda^2}$$

where $v_{f,x}$ and $v_{f,y}$ are the x and y components of the free-flow region fluid velocity v_f, C is the concentration of a given component, H is the height of the flow channel, λ is a dimensionless distance in the y-direction, and D is the diffusion coefficient of the component being considered.

When implementing a finite-element analysis of the system, Huang and Morrissey used a very fine grid spacing near the membrane surface, and lower resolution away from it (because the concentration will change more rapidly near the membrane, as a result of concentration polarization). For simulations modelling the concentration of BSA (a large-diameter solute that would be expected to be rejected by the membrane) in a sodium-chloride solution, they observed a high BSA concentration at the membrane surface, decreasing rapidly in the y direction toward the bulk fluid (the concentration polarization layer was observed to be very thin). For more detailed development of a diffusion-transport model in the membrane context, see, for example, Zunino, 2002.

Note that while changes in the cake resistance, specific cake resistance, available membrane surface area, and local filtration flux over time are considered in the model, these quantities are all represented by "average" values over space. This approach is used consistently throughout the filtration literature, where the emphasis is typically on predicting the overall performance of the system, rather than any local variations. For example, in a real membrane system, the cake layer may develop non-uniformly with respect to the x direction (perhaps thicker near the feed inlet, and thinner away from it), but such variations are typically of less importance to the system operators than the overall flux reduction resulting from the cake layer as a whole.

Any model that attempted to capture the local variations of these quantities would need to be tailored carefully to the particular system being studied (taking into consideration, among other factors, the geometry of the physical membrane

configuration, including the cleaning and aeration mechanisms, which may also not be perfectly uniform along the length of the membrane). Such a model would also change the ordinary differential equations for the cake resistance, specific cake resistance, and available membrane surface area into partial differential equations (because these quantities would now depend on both time and space), so additional boundary conditions and a more complex computational technique would be required. The resulting local filtation flux (for constant-pressure operation) or transmembrane pressure (for constant-flux operation) would then also be functions of space.

Appendix: Membrane Bioreactor Systems

Traditionally, wastewater treatment plants have used activated sludge processes with sedimentation tanks for separating various unwanted particles from the desired clean water stream. However, since the 1990s, there has been a significant trend away from sedimentation and toward membrane bioreactors to achieve this separation (Chang *et al*., 2002).

The figure below provides a simple illustration of a typical membrane bioreactor system (Fitzgerald, 2008). Pre-treated, screened influent enters the bioreactor, where biodegradation takes place. The mixed liquor then flows to the a membrane tank or module placed after the bioreactor. The permeate from the membrane is the treated water; there is continuous recirculation of the mixed liquor (reject stream) between the bioreactor and the membrane tank. A pump applies suction to the inside of the membrane to drive the flow through the membrane. The membrane is continuously aerated, to induce turbulence and remove fouling material as much as possible. The membrane itself can be either hollow-fiber or flat-plate configuration.

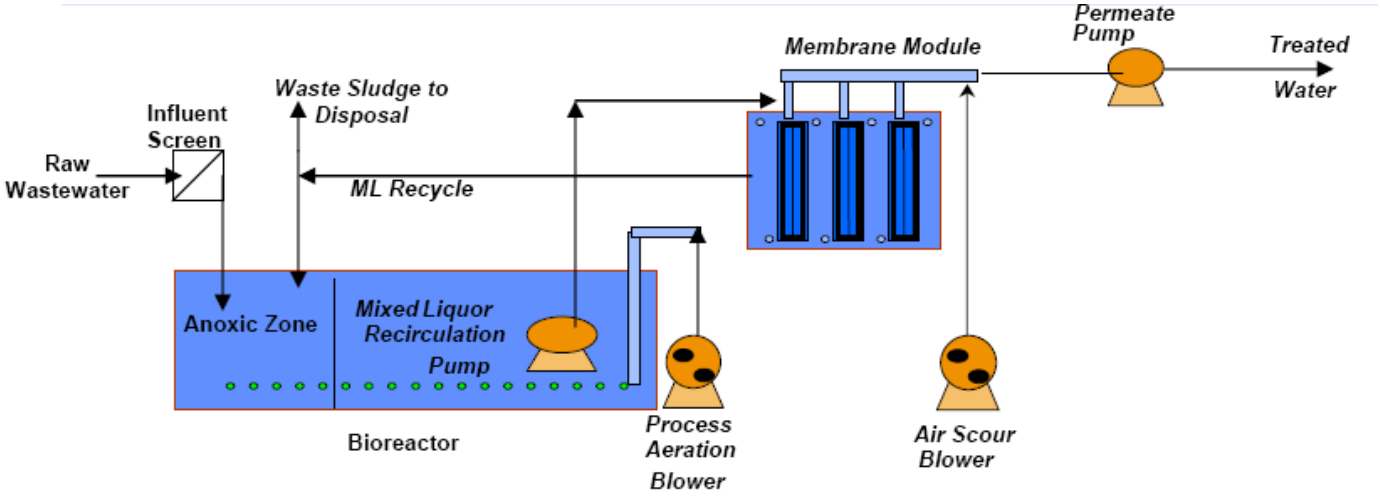

Membrane bioreactors are generally able to provide a cleaner water stream than earlier sedimentation systems, while also having a smaller physical footprint, producing less excess sludge material, and being less prone to process upsets (Drews, 2010). Membrane fouling has consistently been identified as the major challenge in the operation of membrane bioreactor systems – fouling leads to both high capital costs (purchasing new membranes, etc.) and high operating costs (energy costs for aeration, mechanical cleaning, etc.) (Broeckmann *et al*., 2006).

Membranes in these systems are typically backflushed with a chemical cleaner for approximately 15-60s for every 3-12 minutes of filtration time. In addition, they will undergo full maintenance cleanings every 2-7 days, and even more intensive cleanings once or twice a year (Drews, 2010).

Extensive literature is available on the various classes of biological and chemical compounds in wastewater, and their relation to the fouling of membranes (for an overview, see Drews, 2010). However, for macroscopic modelling purposes, it is usually sufficient to assume that the wastewater will contain suspended solids such as sand, pollen, and dyes (which will have a large particle size, and contribute to cake formation), colloidal material (which will have an intermediate particle size, will be microscopically suspended throughout the water stream, and will contribute to pore blocking), and soluble material such as aqueous salts and metal ions (which will have a small particle size, be fully dissolved in the water stream, and will contribute to pore constriction). The proportions of each of these types of material in the wastewater will depend on the source. In addition, the proportions of each type of material in the solution reaching the membrane unit will depend on what (if any) pre-treatment of the water has occurred.

References

V.D. Alves and I.M. Coelhoso. Effect of membrane characteristics on mass and heat transfer in the osmotic evaporation process. *J. Membr. Sci.*, 228(2):159-167, 2004.

American Water Works Association. Microfiltration and ultrafiltration membranes for drinking water. American Water Works Association, Denver, 2005.

A. Beicha and R. Zaamouche. Limiting flux prediction during tubular ultrafiltration. *Chem. Eng. J.*, 153:231-235, 2009.

G. Bolton, D. LaCasse and R. Kuriyel. Combined models of membrane fouling: development and application to microfiltration and ultrafiltration of biological fluids. *J. Membr. Sci.*, 277:75-84, 2006.

A. Broeckmann, J. Busch, T. Wintgens and W. Marquardt. Modeling of pore blocking and cake layer formation in membrane filtration for wastewater treatment. *Desalination*, 189:97-109, 2006.

T.Y. Cath, A.E. Childress and M. Elimelech. Forward osmosis: principles, applications, and recent developments. *J. Membr. Sci.*, 281:70-87, 2006.

I. Chang, J.S. Kim and C.H. Lee. The effects of EPS on membrane fouling in a MBR process. *Proc. MBR3 Conf.*, Cranfield, 19-28, 2001.

I. Chang, P. Le Clech, B. Jefferson and S. Judd. Membrane fouling in membrane bioreactors for wastewater treatment. *J. Env. Eng.*, 128(11):1018-1029, 2002.

N.V. Churaev, R.G. Holdich, P.P. Prokopovich, V.M. Starov and S.I. Vasin. Reversible adsorption inside pores of ultrafiltration membranes. *J. Colloid Interface Sci.*, 288(1):205-212, 2005.

K. Damak, A. Ayadi, B. Zeghmati and P. Schmitz. A new Navier-Stokes and Darcy's law combined model for fluid flow in crossflow filtration tubular membranes. *Desalination*, 161:67-77, 2004.

M. Discacciati and A. Quarteroni. Navier-Stokes/Darcy coupling: modeling, analysis, and numerical approximation. *Rev. Mat. Complut.*, 22(2):315-426, 2009.

E.C. Donaldson, G.V. Chilingarian and T.F. Yen (*editors*). Developments in petroleum science: Enhanced oil recovery, part I: Fundamentals and analyses. Elsevier Science Publishing Company Inc., New York, 1985.

A. Drews. Membrane fouling in membrane bioreactors – characterisation, contradictions, cause and cures. *J. Membr. Sci.*, 363:1-28, 2010.

Environmental Dynamics Inc. Diffuser membrane material selection. Technical bulletin, no date.

A.S. Ferreira and G. Massarani. Physico-mathematical modeling of crossflow filtration. *Chem. Eng. J.*, 111:199-204, 2005.

K.S. Fitzgerald. Membrane bioreactors. Technical report, TSG Technologies, Inc., 2008.

C. Gaucher, P. Jaouen, J. Comiti and P. Legentilhomme. Determination of cake thickness and porosity during cross-flow ultrafiltration on a plane ceramic membrane surface using an electrochemical method. *J. Membr. Sci.*, 210(2):245-258, 2002.

E. Giraldo and M. LeChavallier. Dynamic mathematical modeling of membrane fouling in submerged membrane bioreactors. Technical report, American Water, Innovation and Environmental Stewardship, 2006.

Hach Company. Mixed liquor suspended solids in wastewater. Technical document, no date.

N.S. Hanspal, A.N. Waghode, V. Nassehi and R.J. Wakeman. Development of a predictive mathematical model for coupled Stokes/Darcy flows in cross-flow membrane filtration. *Chem. Eng. J.*, 149:132-142, 2009.

L. Huang and M.T. Morrissey. Finite element analysis as a tool for crossflow membrane filter simulation. *J. Membr. Sci.*, 155:19-30, 1999.

K. Hwang and P. Sz. Filtration characteristics and membrane fouling in cross-flow microfiltration of BSA/dextran binary suspension. *J. Membr. Sci.*, 347:75-82, 2010.

D. Jeison and J.B. van Lier. Cake layer formation in anaerobic submerged membrane bioreactors (AnSMBR) for wastewater treatment. *J. Membr. Sci.*, 284:227-236, 2006.

J.S. Kim, C.H. Lee and I.S. Chang. Effect of pump shear on the performance of a crossflow membrane bioreactor. *Water Res.*, 35:2137-2144, 2001.

J. Kinčl, P. Določek and J. Cakl. Filtration model for hollow fiber membranes with compressible cake formation. *Desalination*, 240:99-107, 2009.

Z. Li, T. Katsumi and T. Inui. Modeling cake filtration under coupled hydraulic, electric and osmotic effects. *J. Membr. Sci.*, 378:485-494, 2011.

Millipore Corporation. Protein concentration and diafiltration by tangential flow filtration. Technical brief, 2003.

J.M. Miranda and J.B.L.M. Campos. Mass transfer in the vicinity of a separation membrane – the applicability of the stagnant film theory. *J. Membr. Sci.*, 202:137-150, 2002.

M. Ousman and M. Bennasar. Determination of various hydraulic resistances during cross-flow filtration of a starch grain suspension through inorganic membranes. *J. Membr. Sci.*, 105:1-21, 1995.

S.I.S. Pinto, J.M. Miranda and J.B.L.M. Campos. Numerical study of the effect of a charged membrane in the separation of electrically charged components. *Desalination and Water Treatment*, 14:201-207, 2010.

S. Ri, Z. Zhang, L. Chi and W. Zhou. Blocking filtration model of microfiltration membrane separation for non-Newtonian fluid solution. Technical report, Shanghai Jiaotong University, no date.

M. Saleem, R.U. Khan, M.S. Tahir and G. Krammer. Experimental study of cake formation on heat treated and membrane coated needle felts using optical in-situ cake height measurement. *Powder Technology*, 214(3):388-399, 2011.

L. Song. Flux decline in crossflow microfiltration and ultrafiltration: mechanisms and modeling of membrane fouling. *J. Membr. Sci.*, 139:183-200, 1998.

United States Environmental Protection Agency, Office of Water. Membrane filtration guidance manual. Technical document, 2005.

M.C.V. Vela, S.Á. Blanco, J.L. García and E.B. Rodríguez. Analysis of membrane pore blocking models adapted to crossflow ultrafiltration in the ultrafiltration of PEG. *Chem. Eng. J.*, 149:232-241, 2009.

P.A. Vesilind, J.J. Peirce and R.F. Weiner. Environmental engineering (3rd revised edition). Butterworth-Heinemann Ltd., London, 1994.

H.K. Vyas, A.J. Mawson, R.J. Bennett and A.D. Marshall. A new method for estimating cake height and porosity during crossflow filtration of particulate suspensions. *J. Membr. Sci*., 176(1):113-119, 2000.

L.K. Wang. Handbook of industrial and hazardous wastes treatment. Marcel Dekker Incorporated, New York, 2004.

Weise Water Systems. Frequently asked questions to membrane bioreactors in general. Online document, 2010.

J. Wu, C. He, X. Jiang and M. Zhang. Modeling of the submerged membrane bioreactor fouling by the combined pore constriction, pore blockage and cake formation mechanisms. *Desalination*, 279:127-134, 2011.

Y. Ye, P. LeClech, V. Chen, A.G. Fane and B. Jefferson. Fouling mechanisms of alginate solutions as model extracellular polymeric substances. *Desalination*, 175:7-20, 2005.

P. Zunino. Mathematical and numerical modeling of mass transfer in the vascular system. Ph.D. thesis, École Polytechnique Fédérale de Lausanne, 2002.